STUDY OF THE INJECTION UPSETTING OF METALS

B. Parsons* P. R. Milner† B. N. Cole‡

The punch pressure required to injection upset a cylindrical billet of an isotropic, non-work-hardening, rigid–plastic material is derived using an upper bound (velocity field) technique and by a 'slab' stress analysis. A method for applying the theory to the injection upsetting of work-hardening materials is evolved and the validity of this application is demonstrated by the results of experiments using pure aluminium, an aluminium alloy and copper.

1 INTRODUCTION

INJECTION UPSETTING is essentially the production of a localized increase in the diameter of part of a cylindrical billet of plastically deformable material by forcing the material to flow into an annular space of fixed clearance (see Fig. 1). Experimental studies of this process by the N.E.L. (National Engineering Laboratory) (1) (2)§ have shown that for various steels a larger volume of flange can be produced by this method than by the more conventional processes of heading or flange forging. In the latter process, the volume of the resulting flange is restricted by buckling of the initially unrestrained portion of the billet, which tends to occur when this exceeds 2·5 times the billet diameter.

Other work on injection upsetting has been concerned with the cold forming of flanges on billets of materials having limited ductility by performing the operation against a constraining hydrostatic pressure (3)–(6). It has been shown that a hydrostatic constraining pressure applied to the flange rim increases the limiting diameter of the flange that can be formed on billets of both ductile and brittle metals.

Although complete theoretical solutions are known for certain problems of the flow of a rigid–plastic body (7) (8), such solutions are generally difficult to obtain and, in recent published work, much use has been made of partial solutions satisfying the upper bound theorem given by Hill (9). Such solutions involve the derivation of a kinematically admissible velocity field and may often be obtained easily by the methods of Johnson (10) or Kudo (11) (12). Many examples of analysis of metal forming processes may be found, e.g. in (13) (14). The corresponding lower bound theorem consists of deriving a statically admissible stress field for the deforming body. The conditions of the theorem are relatively difficult to satisfy and some simplification of the equilibrium equations is usually necessary to obtain an analysis of the stresses in the deforming body. Most stress analyses therefore yield an approximate value for the work rate and tool pressures, rather than a lower bound. Avitzur (13) (15) has produced lower bounds for forging between rough, parallel platens.

The MS. of this paper was received at the Institution on 12th February 1973 and accepted for publication on 9th August 1973. 33

* *Senior Lecturer, Department of Mechanical Engineering, The University of Leeds, Leeds LS2 9JT. Member of the Institution.*

† *Lecturer, Department of Mechanical Engineering, Teesside Polytechnic, Middlesbrough TS1 3BA. Graduate Member of the Institution.*

‡ *Professor of Mechanical Engineering and Head of Department, Department of Mechanical Engineering, The University of Leeds. Fellow of the Institution.*

§ *References are given in Appendix 3.*

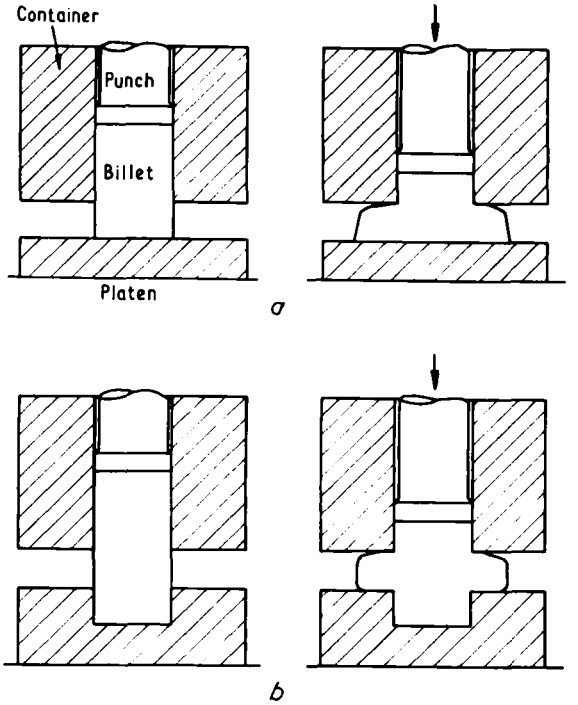

a On the end of a billet.
b Part way along the billet.

Fig. 1. *The injection upsetting process*

Existing lower bounds for more complex forming processes are derived from 'ideal' deformation, disregarding friction and internal shearing effects. These usually underestimate the actual tool forces by a considerable margin.

Useful theoretical analyses of injection upsetting are still largely lacking. Cogan and Dorman (5) presented several analyses, none of which predicts the observed variation in punch pressures required for upsetting flanges of different thicknesses on a given diameter billet. The upper bound analysis of Alexander and Lengyel (6) does predict these pressure variations, but the present work indicates that their solution greatly overestimates the punch pressure, particularly for the production of thin flanges. The method for allowing for work-hardening as introduced by Alexander *et al.* is, in the present work, used in a modified form so as to take into account the non-steady nature of the upsetting process.

1.1 Notation

a	Billet radius.
b	Nominal flange thickness.

$\dot{e}_{rr}, \dot{e}_{zz}, \dot{e}_{\theta\theta}, \dot{e}_{rz}, \dot{e}_{zr}$	Strain rates (axial symmetry).
m	Friction factor ($0 \leqslant m \leqslant 1$).
p	Mean punch pressure.
p (with suffixes)	Partial punch pressure, i.e. separate contributions of various effects to the total mean punch pressure.
q	Radial pressure applied to rim of flange.
r, z, θ	Cylindrical co-ordinates.
R_0	$= r_0/a$.
R	$= r/a$.
r_0	Flange outer radius.
U	Punch velocity.
u_r, u_z	Flow velocities.
v (with suffixes)	Slip velocity along a surface of flow discontinuity.
$\dot{W}$	Rate of working of punch or, with suffixes, separate contributions to $\dot{W}$.
λ	Geometrical parameter defining the axial extent of the deformation zone within the billet.
ρ	$= b/a$.
σ_0	Yield or flow stress of the deforming material.
$\sigma_r, \sigma_\theta, \sigma_z$	Direct stresses (axial symmetry).
τ_{rz}, τ_{zr}	Shear stresses (axial symmetry).

Other symbols, which are not used extensively in the analysis, will be defined as required.

2 THE BASIC EQUATIONS OF STRESS AND FLOW FOR AXISYMMETRIC DEFORMING BODIES

The following equations are presented in a form relevant to the subsequent analysis; typical derivations may be found in (13) (14).

Continuity of flow:

$$\frac{\partial u_z}{\partial z} = -\frac{1}{r}\frac{\partial}{\partial r}(ru_r) \quad . \quad . \quad . \quad . \quad (1)$$

Strain rates:

$$\left.\begin{aligned} \dot{e}_{rr} &= \frac{\partial u_r}{\partial r} \qquad \dot{e}_{zz} = \frac{\partial u_z}{\partial z} \qquad \dot{e}_{\theta\theta} = \frac{u_r}{r} \\ \dot{e}_{rz} &= \dot{e}_{zr} = \frac{1}{2}\left(\frac{\partial u_r}{\partial z} + \frac{\partial u_z}{\partial r}\right) \end{aligned}\right\} . \quad (2)$$

Radial static equilibrium:

$$\frac{\partial \sigma_r}{\partial r} + \frac{\partial \tau_{rz}}{\partial z} + \frac{\sigma_r - \sigma_\theta}{r} = 0 \quad . \quad . \quad . \quad (3)$$

Axial static equilibrium:

$$\frac{\partial \sigma_z}{\partial z} + \frac{\partial \tau_{rz}}{\partial r} + \frac{\tau_{rz}}{r} = 0 \quad . \quad . \quad . \quad . \quad (4)$$

Yield (von Mises):

$$\sigma_0^2 = \tfrac{1}{2}\{(\sigma_r - \sigma_\theta)^2 + (\sigma_\theta - \sigma_z)^2 + (\sigma_z - \sigma_r)^2 + 6\tau_{rz}^2\} \quad (5)$$

Rate of working due to deformation within volume V*:*

$$\dot{W}_i = \frac{2\sigma_0}{\sqrt{3}} \int_V \sqrt{(\sum \tfrac{1}{2}\dot{e}_{ij}\dot{e}_{ij}\, dV)} \quad . \quad . \quad (6)$$

where $i, j = r, z, \theta$.

Rate of working due to slip on a surface of flow discontinuity (area A*) within the deforming body:*

$$\dot{W}_s = \frac{\sigma_0}{\sqrt{3}} \int_A |v|\, dA \quad . \quad . \quad . \quad (7)$$

Equations (6) and (7) apply strictly to an isotropic, non-work-hardening rigid–plastic material obeying the von Mises yield criterion (i.e. a Lévy–Mises material). However, a mean value of σ_0 for a work-hardening material may be derived from an upper bound solution for an ideal plastic material and the upper bound analysis may then be applied to the work-hardening case.

3 A MINIMIZED UPPER BOUND ON POWER FOR INJECTION UPSETTING

In the following analysis, an upper bound solution is developed in which $\dot{W}$ is minimized with respect to the position of the surface of velocity discontinuity that divides the deforming part of the billet from the undeformed part (regions 1 and 2 in Fig. 2*a*). This discontinuity surface is assumed to be conical and, given this

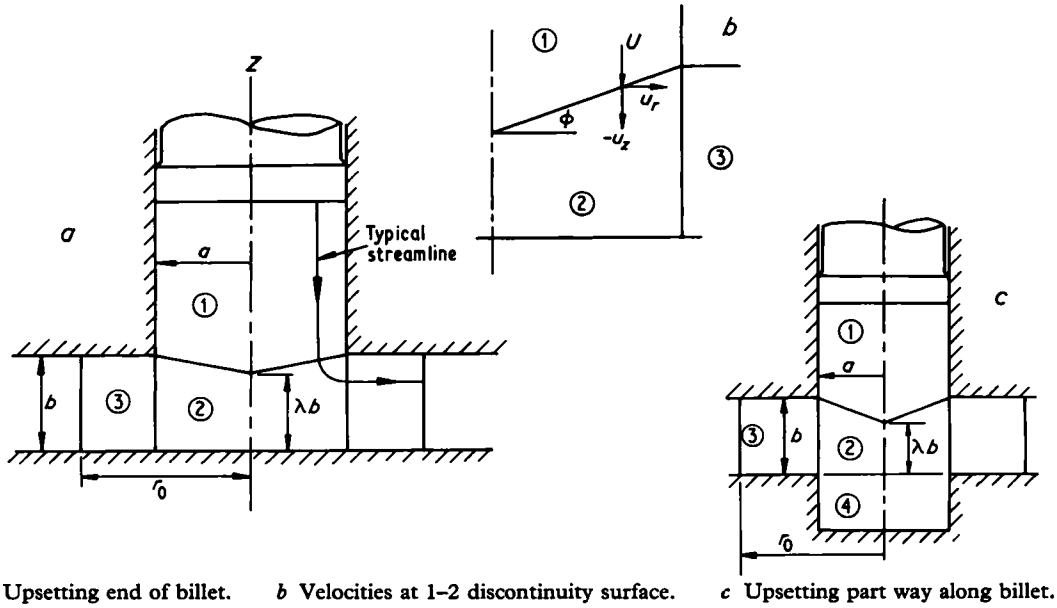

a Upsetting end of billet. *b* Velocities at 1–2 discontinuity surface. *c* Upsetting part way along billet.

Fig. 2. *Partitioning of deforming material for theoretical analysis*

variational restriction on the extent of the plastic region, it is not possible therefore to achieve a complete solution. The values of $\dot{W}$ derived in this manner are therefore overestimates of the correct value by an unknown margin.

The deforming body is resolved into three distinct regions, as shown in Fig. 2*a*. In region 1, the material is rigid and is moving axially at the punch velocity U. Region 3 is a zone of purely radial flow (in practice, axial contraction of the flange occurs unless a sufficiently large radial pressure is applied to the flange rim, but disregard of this effect has been shown (**16**) to cause an error in the value of the mean punch pressure which is not greater than, and is probably much less than, $+0{\cdot}19\sigma_0$). The radial velocity in region 3 is assumed to be independent of z and so continuity from region 1 to a cylindrical surface of radius r in region 3 requires that, at that surface

$$u_r = \frac{Ua^2}{2br} \quad . \quad . \quad . \quad . \quad . \quad . \quad (8)$$

In region 2, equation (1) must be satisfied throughout. In addition, the velocity field must satisfy continuity requirements at the boundaries dividing this region from regions 1 and 3. These conditions alone are insufficient to define u_z and u_r uniquely throughout region 2; it may be noted, however, that u_r is independent of z in region 3 and if this condition is extended to region 2, the solution of equation (1) is greatly simplified and is unique. The velocity field for this region is derived in Appendix 1, where it is shown that

$$u_r = \frac{Uar}{2b[\lambda a + r(1-\lambda)]}, \qquad u_z = -\frac{Uaz}{2b}\left[\frac{2\lambda a + r(1-\lambda)}{[\lambda a + r(1-\lambda)]^2}\right] \quad . \quad . \quad . \quad (9)$$

The strain rates for region 2 are found from equation (2) and are given by

$$\left.\begin{aligned} \dot{e}_{rr} &= \frac{U\lambda a^2}{2b[\lambda a + r(1-\lambda)]^2} \qquad \dot{e}_{\theta\theta} = \frac{Ua}{2b[\lambda a + r(1-\lambda)]} \\ \dot{e}_{zz} &= -\frac{Ua}{2b}\left[\frac{2\lambda a + r(1-\lambda)}{[\lambda a + r(1-\lambda)]}\right] \\ \dot{e}_{rz} &= \dot{e}_{zr} = \frac{Uaz\{1-\lambda\}\{3\lambda a + r(1-\lambda)\}}{4b[\lambda a + r(1-\lambda)]^3} \end{aligned}\right\} \quad (10)$$

and for region 3,

$$\dot{e}_{rr} = -\frac{Ua^2}{2br^2} \quad \dot{e}_{\theta\theta} = \frac{Ua^2}{2br^2} \quad \dot{e}_{zz} = \dot{e}_{zr} = \dot{e}_{rz} = 0 \quad (11)$$

In the calculations of $\dot{W}$, account must be taken of the shear work performed at the 1–2 and 2–3 boundaries, where velocity discontinuities tangential to these boundaries exist. On the 2–3 boundary, the slip velocity (v_{23}) is simply the difference between the values of u_z, at $r = a$, for the two regions, thus

$$|v_{23}| = \frac{Uz(\lambda+1)}{2b} \quad . \quad . \quad . \quad (12)$$

Using the notation of Fig. 2*b*, the slip velocity on the 1–2 boundary is given by

$$|v_{12}| = U\sin\phi + u_r\cos\phi + u_z\sin\phi \quad . \quad (13)$$

It may be verified that

$$|v_{12}| = \frac{Ur\sqrt{[a^2+b^2(1-\lambda)^2]}}{2b[\lambda a + r(1-\lambda)]} \quad . \quad . \quad (14)$$

$\dot{W}$ and hence the mean punch pressure can now be derived using equations (6) and (7). For region 3, the rate of working due to internal deformation ($\dot{W}_{I3}$) is given by

$$\dot{W}_{I3} = \frac{2\sigma_0}{\sqrt{3}}\int_a^{r_0}\frac{1}{\sqrt{2}}\sqrt{\left(\frac{U^2a^4}{4b^2r^4}+\frac{U^2a^4}{4b^2r^4}\right)}\,2\pi r\,\mathrm{d}r = \frac{2\pi a^2 U\sigma_0}{\sqrt{3}}\ln\frac{r_0}{a} \quad (15)$$

For region 2, the internal power of deformation ($\dot{W}_{I2}$) may be derived very simply when $\lambda = 1$, but for the general case numerical integration of equation (6) is necessary. It may be verified that

$$\sum \tfrac{1}{2}\dot{e}_{ij}\dot{e}_{ij} = \frac{U^2a^2}{4b^2}\left\{\frac{3\lambda^2a^2+3ar\lambda+3ar\lambda^2+r^2-2r^2\lambda+r^2\lambda^2}{[\lambda a+r(1-\lambda)]^4}\right\} + \frac{U^2a^2z^2}{16b^2}\left\{\frac{(1-\lambda)^2[3a\lambda+r(1-\lambda)]^2}{[\lambda a+r(1-\lambda)]^6}\right\} \quad (16)$$

On substitution of equation (16) into equation (6), the integration with respect to z can be executed simply. The integration with respect to r was performed numerically and the resulting values of $\dot{W}_{I2}$ are tabulated in Appendix 2.

The power due to shear at the 1–2 boundary ($\dot{W}_{s12}$) is given by equations (7) and (14):

$$\dot{W}_{s12} = \frac{U\sigma_0}{\sqrt{3}}\int_0^a \frac{r\sqrt{[a^2+b^2(1-\lambda)^2]}}{2b[\lambda a+r(1-\lambda)]}\cdot\frac{\sqrt{[a^2+b^2(1-\lambda)^2]}}{a} \times 2\pi r\,\mathrm{d}r$$

and hence

$$\dot{W}_{s12} = \frac{\pi a^2\sigma_0 U[1+\rho^2(1-\lambda)^2]}{\rho(1-\lambda)\sqrt{3}}\left\{\frac{1}{2}-\frac{\lambda}{1-\lambda}+\frac{\lambda^2}{(1-\lambda)^2}\ln\frac{1}{\lambda}\right\} \quad . \quad . \quad . \quad (17)$$

Equation (17) may be rewritten in the series form:

$$\dot{W}_{s12} = \frac{\pi a^2\sigma_0 U[1+\rho^2(1-\lambda)^2]}{\rho\sqrt{3}} \times\left\{\frac{1}{3\lambda}-\frac{(1-\lambda)}{4\lambda^2}+\frac{(1-\lambda)^2}{5\lambda^3}-\cdots\right\} \quad (18)$$

which is valid for all $\lambda > 0{\cdot}5$. This facilitates the computation of $\dot{W}_{s12}$ when λ is close to unity.

The rate of working due to shear at the 2–3 boundary ($\dot{W}_{s23}$) is, from equations (7) and (12):

$$\dot{W}_{s23} = \frac{U\sigma_0}{\sqrt{3}}\int_0^b\frac{(\lambda+1)z}{2b}2\pi a\,.\,\mathrm{d}z = \frac{\pi a^2\sigma_0 U(\lambda+1)}{2\sqrt{3}} \quad (19)$$

The total rate of working is the sum of the component parts above, thus

$$\dot{W} = \dot{W}_{s12}+\dot{W}_{I2}+\dot{W}_{s23}+\dot{W}_{I3} \quad . \quad . \quad (20)$$

and the mean punch pressure is given by

$$\frac{p}{\sigma_0} = \frac{\dot{W}}{\pi a^2\sigma_0 U}+\frac{q}{\sigma_0}$$

where q is the restraining pressure applied at the flange rim.

(The individual contributions to p are denoted by

$$\frac{p_{s12}}{\sigma_0} = \frac{\dot{W}_{s12}}{\pi a^2\sigma_0 U}, \qquad \frac{p_{I2}}{\sigma_0} = \frac{\dot{W}_{I2}}{\pi a^2\sigma_0 U}, \quad \text{etc.}$$

and are referred to as partial punch pressures.)

Thus, the non-dimensional punch pressure p/σ_0 can be expressed as

$$\frac{p}{\sigma_0} = F(\rho,\lambda)+\frac{2}{\sqrt{3}}\ln R_0+\frac{q}{\sigma_0} \quad . \quad . \quad (21)$$

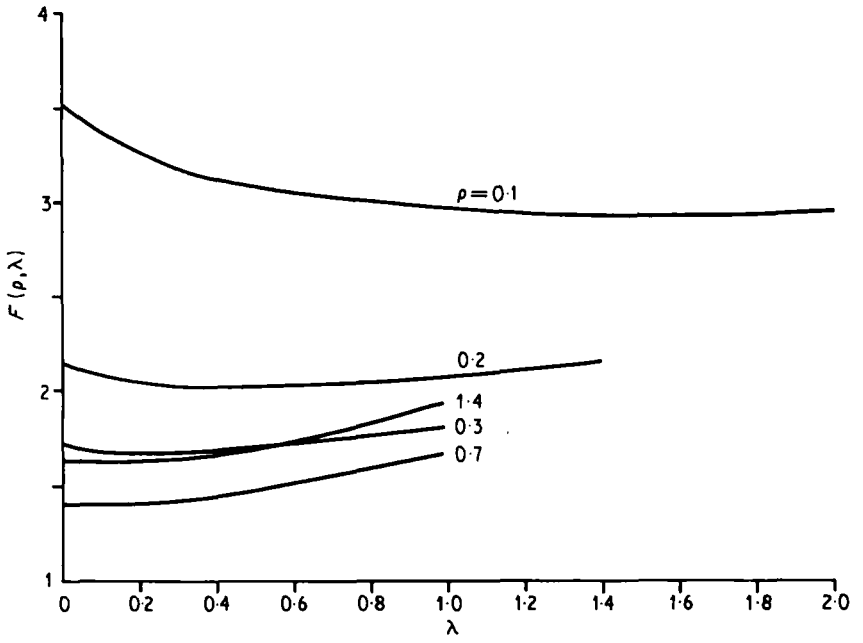

Fig. 3. *Variation of the λ-dependent component of punch pressure for various values of ρ*

where $F(\rho, \lambda) = \frac{p_{I2}}{\sigma_0} + \frac{p_{s12}}{\sigma_0} + \frac{p_{s23}}{\sigma_0}$, and $R_0 = \frac{r_0}{a}$

The function $F(\rho, \lambda)$ is shown in Fig. 3. The minima of the curves represent the optimum upper bound for a given value of ρ; the value of λ for which this occurs is denoted by λ_{opt}. A table of $F(\rho, \lambda_{opt})$ and its components is given in Table 1, and the variation of punch pressure with R_0 is shown for the case $q = 0$ in Fig. 4.

The upper bound solution derived by Alexander and Lengyel (**6**) is

$$\frac{p}{\sigma_0} = \frac{1}{\sqrt{3}} + \frac{4}{3\rho\sqrt{3}} + \frac{\rho}{\sqrt{3}} + \frac{2}{\sqrt{3}} \ln R_0 + \frac{q}{\sigma_0} \quad (22)$$

The solutions (21) and (22) are compared in Fig. 5. Also shown is a simple upper bound obtained by using the foregoing analysis with $\lambda = 1$. This leads to the equation:

$$\frac{p}{\sigma_0} = 1 + \frac{1}{3\rho\sqrt{3}} + \frac{\rho}{\sqrt{3}} + \frac{2}{\sqrt{3}} \ln R_0 \frac{q}{\sigma_0} \quad . \quad (23)$$

The curve given by equation (23) touches the optimized upper bound at $\rho \simeq 0{\cdot}13$ and, by comparison of equations (22) and (23), it may be shown that when $R_0 = 1$, equation

Table 1. *Function $F(\rho, \lambda_{opt})$ for flange at end of billet*

ρ	λ_{opt}	$\frac{W_{I2}}{\pi a^2 \sigma_0 U}$	$\frac{W_{s12}}{\pi a^2 \sigma_0 U}$	$\frac{W_{s23}}{\pi a^2 \sigma_0 U}$	$\frac{p}{\sigma_0}\left(\frac{r_0}{a}=1\right)$
0·06	3·70	1·637	2·143	0·082	3·862
0·08	2·33	1·357	1·896	0·077	3·330
0·10	1·59	1·182	1·695	0·075	2·952
0·14	0·89	0·966	1·411	0·077	2·454
0·18	0·55	0·836	1·227	0·080	2·143
0·20	0·45	0·795	1·149	0·084	2·028
0·30	0·21	0·689	0·886	0·105	1·680
0·40	0·12	0·647	0·743	0·129	1·519
0·50	0·08	0·629	0·656	0·156	1·441
0·60	0·06	0·621	0·604	0·184	1·409
0·80	0·06	0·629	0·538	0·245	1·412
1·00	0·07	0·645	0·509	0·309	1·463
1·20	0·07	0·657	0·512	0·370	1·539
1·40	0·08	0·676	0·515	0·437	1·628
1·60	0·11	0·711	0·504	0·512	1·727

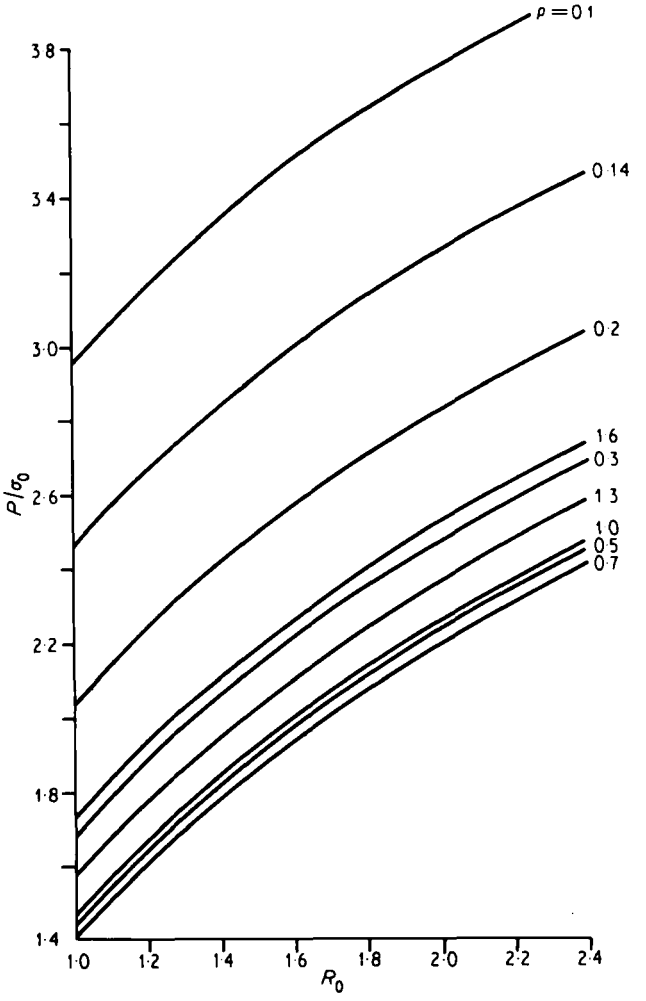

Fig. 4. *Variation of punch pressure with flange radius for differing values of ρ*

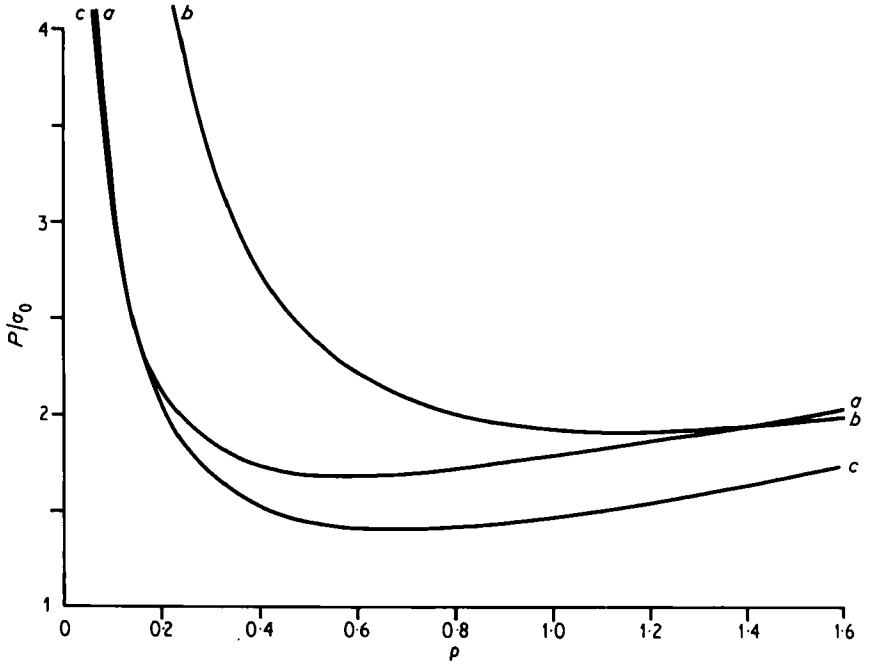

a Simple upper bound ($\lambda = 1$).
b Alexander and Lengyel (**6**).
c Upper bound optimized with respect to λ.

Fig. 5. *Comparison of upper bound solutions* ($q = 0$)

(21) must lead to values of p/σ_0 which are somewhat less than a quarter of those given by equation (23) for values of ρ approaching zero.

Frictional effects between workpiece and tooling can be accounted for theoretically if the surface shear stress is assumed to be a constant factor m (where $0 \leqslant m \leqslant 1$) of the material shear strength. The power dissipated and the partial punch pressures due to frictional effects may then be calculated by using equation (7) and replacing σ_0 by $m\sigma_0$. Since the calculations are essentially similar to the foregoing, only the results are given. The partial punch pressures due to frictional effects are: between billet and container in region 1, where l is the billet length in the container

$$\frac{p_{s1}}{\sigma_0} = \frac{2ml}{a\sqrt{3}} \quad . \quad . \quad . \quad . \quad . \quad (24)$$

and at the platen surface in region 2,

$$\frac{p_{s2}}{\sigma_0} = \frac{m}{\rho(1-\lambda)\sqrt{3}} \left\{ \frac{1}{2} - \frac{\lambda}{1-\lambda} + \frac{\lambda^2}{(1-\lambda)^2} \ln \frac{1}{\lambda} \right\} . \quad (25)$$

In region 3, the frictional work will depend on whether or not a restraining radial pressure q is applied to the flange rim. As a result of axial thinning, if $q = 0$, then contact between the flange and the tooling will only occur at the lower platen. If, for a first approximation, it is assumed that the radial extent of this contact is given by $r'_0 = a+b$, then the partial punch pressure due to this effect will be

$$\frac{p_{s3}}{\sigma_0} = \frac{m}{\sqrt{3}} \quad . \quad . \quad . \quad . \quad . \quad . \quad (26)$$

If a radial pressure q is applied and is sufficient to prevent axial thinning, then

$$\frac{p_{s3}}{\sigma_0} = \frac{2m}{\rho\sqrt{3}}(R_0 - 1) \quad . \quad . \quad . \quad (27)$$

Putting $m = 1$ into equation (25) produces the additional term necessary in $F(\rho, \lambda)$ to produce an upper bound for injection of a flange part way along the billet (Fig. 2*c*). For this case the velocity field is unchanged, but there is now a dead zone 4 and a slip plane between region 2 and 4. Table 2 gives $F(\rho, \lambda_{opt})$ for this case and the variation of this function for $m = 0$ and $m = 1$ is shown in Fig. 6. The introduction of the p_{s2} term into equation (21) increases the value of λ_{opt} and p_{s2} is therefore not exactly linearly dependent on m. However, the error produced by linear interpolation between the $m = 0$ and $m = 1$ curves is negligible.

Application of the above theory to a work-hardening material requires the replacement of the constant flow stress σ_0 of the ideal plastic material by a mean flow stress appropriate to the particular material in question. This is achieved using the upper bound solution for the ideal plastic as follows. When the punch moves downwards for a time δt, it moves a distance $U\,\delta t$ and each elemental disc of undeformed billet that has previously entered regions 2 and 3 is distorted as it progresses in these regions through a small distance that could be derived from the

Table 2. *Function* $F(\rho, \lambda_{opt})$ *for flange part way along billet*

ρ	λ_{opt}	$\frac{p_{12}}{\sigma_0}$	$\frac{p_{s12}}{\sigma_0}$	$\frac{p_{s23}}{\sigma_0}$	$\frac{p_{s24}}{\sigma_0}$	$\frac{p}{\sigma_0}$
0·10	3·80	1·667	1·337	0·139	1·240	4·383
0·18	1·55	1·169	0·958	0·132	0·947	3·206
0·30	0·72	0·901	0·698	0·148	0·692	2·439
0·40	0·27	0·720	0·664	0·147	0·613	2·134
0·50	0·26	0·718	0·559	0·182	0·491	1·950
0·60	0·24	0·712	0·499	0·215	0·413	1·839
0·80	0·21	0·707	0·440	0·279	0·315	1·741
1·00	0·18	0·704	0·428	0·341	0·256	1·729
1·20	0·18	0·717	0·419	0·409	0·213	1·758
1·40	0·18	0·732	0·423	0·477	0·183	1·815
1·60	0·19	0·754	0·426	0·549	0·160	1·889

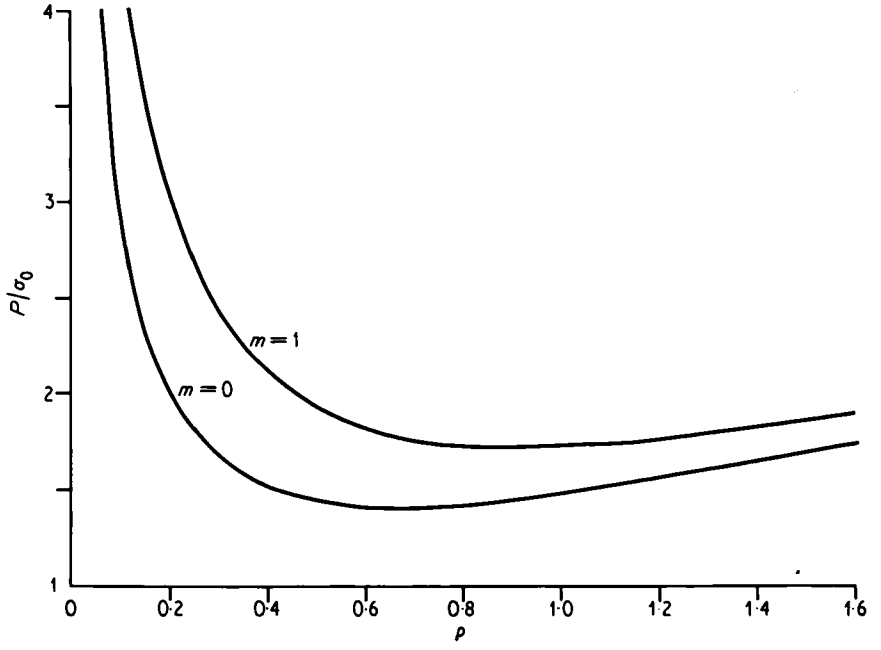

Fig. 6. *Optimized upper bound solutions assuming friction of platen surface ($q = 0$)*

velocity equations. Since the velocity field is time-independent, the incremental work done by the punch is equal to that required to propel one such elemental disc from region 1 into regions 2 and 3 until it reached the instantaneous extremity of region 3. If the mean effective strain imparted on the disc during such a movement is $\bar{e}_m$, then the work done/unit volume of material is $\sigma_{0m}\bar{e}_m$, where σ_{0m} is the mean effective flow stress. Thus, the work done (δW) by the punch in time δt is

$$\delta W = \pi a^2 U\, \delta t . \sigma_{0m}\bar{e}_m$$

or

$$\frac{\mathrm{d}W}{\mathrm{d}t} = \dot{W} = \pi a^2 U \sigma_{0m}\bar{e}_m$$

that is

$$\frac{p}{\sigma_{0m}} = \bar{e}_m \quad . \quad . \quad . \quad . \quad . \quad . \quad . \quad (28)$$

The above equation should exclude external frictional work done, as this work is not dissipated within the material as bulk plastic straining. Thus, equation (28) indicates that in the frictionless upper bound solution, if σ_0 is replaced by σ_{0m}, the mean effective strain ($\bar{e}_m$) associated with the process becomes equal to the right-hand side of the punch pressure equation (21). This can be calculated and from a true stress–true strain curve for the material concerned, σ_{0m} may be found using the relationship:

$$\sigma_{0m} = \frac{1}{\bar{e}_m}\int_0^{\bar{e}_m} \sigma_0 \, \mathrm{d}\bar{e} \quad . \quad . \quad . \quad . \quad (29)$$

and so p may be estimated. It is evident that for a continuously work-hardening material, $\bar{e}_m$ and σ_{0m} will be overestimated by an amount that is dependent on the accuracy of the upper bound solution used. In using the upper bound solution to find p, having estimated σ_{0m}, the total error is increased further and so to be able to apply the theory with confidence to the forming of rapidly work-hardening materials, it is desirable to obtain as accurate an upper bound as possible.

The above derivation of $\bar{e}_m$ contains the assumption that all the material in regions 2 and 3 originated in region 1 and the results were used as such by Alexander and Lengyel. Since region 2 is initially filled with undeformed material, which will not undergo the deformations associated with crossing the 1–2 boundary, and to some extent those associated with movement through region 2, it is perhaps more correct to assume that the actual $\bar{e}_m$ in some factor $\phi(R_0)$ of the value derived above, where ϕ is a monotone increasing function of R_0 which takes the value zero when $R_0 = 1$ and unity as R_0 tends to infinity. A suitable function satisfying these requirements is

$$\phi = \frac{R_0 - 1}{R_0 - k}, \quad (0 < k < 1)$$

and using this

$$\bar{e}_m = \frac{R_0 - 1}{R_0 - k} \cdot \frac{p}{\sigma_{0m}} \quad . \quad . \quad . \quad . \quad (30)$$

where p/σ_{0m} is given by the right-hand side of equation (21) using appropriate values of $F(\rho, \lambda_{opt})$ from either Table 1 or Table 2.

4 AN ELEMENTARY STRESS ANALYSIS

The deforming billet is partitioned as in Fig. 2*a* with $\lambda = 1$ and with surface frictional stresses ($m\sigma_0/\sqrt{3}$) at all points of contact with the tooling. The flow discontinuity surface between regions 1 and 2 indicated by the velocity field is assumed to result in a restraint on the radial movement of material in region 2; a radial internal friction stress of value ($\sigma_0/\sqrt{3}$) acts on the upper surface of this region. The method of analysis chosen cannot accommodate the similar restraint resulting from the discontinuity of axial velocity at the 2–3 boundary. The stress analysis is simplified by disregarding the effects of the shear tractions on the internal equilibrium of the deforming body. These shear tractions are taken to appear as axially uniform radial body forces in regions 2 and 3, and radially uniform axial body forces in region 1. Additionally, in regions 2 and 3, σ_θ and σ_r are assumed to be axially uniform and therefore the term in τ_{rz} disappears from equation (3) and equation (4) becomes redundant.

With the above assumptions it is found that the Lévy–Mises equations are satisfied piecewise within regions 2 and 3 and the associated velocity fields for these regions are given by putting $\lambda = 1$ into the relevant expression of Table 1. Because the Lévy–Mises relationships are not continuously satisfied throughout regions 2 and 3 and also because of the simplifications in the equilibrium conditions, the following solution is not a lower bound.

The simplified radial equilibrium equation for region 3 is

$$\frac{d\sigma_r}{dr}+\frac{\sigma_r-\sigma_\theta}{r}-\frac{2m\sigma_0}{b\sqrt{3}}=0 \quad . \quad . \quad . \quad (31)$$

Axial thinning is disregarded and the plane strain yield criterion:

$$\sigma_\theta-\sigma_r=\frac{2\sigma_0}{\sqrt{3}} \quad . \quad . \quad . \quad . \quad (32)$$

applies. Combining equations (31) and (32), integrating and inserting the boundary conditions $\sigma_r = -q$ on $r = r_0$ gives:

$$\left.\begin{aligned}\sigma_r &= -\frac{2\sigma_0}{\sqrt{3}}\left[\ln\frac{r_0}{r}+\frac{m}{b}(r_0-r)\right]-q \\ \text{or}\qquad \sigma_r &= -\frac{2\sigma_0}{\sqrt{3}}\left[\ln\frac{R_0}{R}+\frac{m}{\rho}(R_0-R)\right]-q\end{aligned}\right\} \quad (33)$$

In plane strain, $\sigma_z=\dfrac{\sigma_\theta+\sigma_r}{2}$

Therefore,

$$\sigma_\theta = -\frac{2\sigma_0}{\sqrt{3}}\left[\ln\frac{R_0}{R}+\frac{m}{\rho}(R_0-R)-1\right]-q \quad (34)$$

and

$$\sigma_z = -\frac{2\sigma_0}{\sqrt{3}}\left[\ln\frac{R_0}{R}+\frac{m}{\rho}(R_0-R)-\tfrac{1}{2}\right]-q \quad (35)$$

The yield criterion for region 2 may be obtained by an appeal to the Lévy–Mises equations, the general yield equation (5) and the strain rate equations (10) with $\lambda = 1$. Equations (10) reduce to

$$\dot{e}_{rr}=\dot{e}_{\theta\theta}=\frac{U}{2b} \qquad \dot{e}_{zz}=-\frac{U}{b} \qquad \dot{e}_{rz}=\dot{e}_{zr}=0 \quad (36)$$

The Lévy–Mises relationships then require that equation (5) reduce to

$$\sigma_\theta=\sigma_r=\sigma_0+\sigma_z \quad . \quad . \quad . \quad (37)$$

Radial equilibrium in region 2 requires that

$$\frac{d\sigma_r}{dr}-\frac{(1+m)\sigma_0}{b\sqrt{3}}=0 \quad . \quad . \quad . \quad . \quad (38)$$

The arbitrary constant is found by equating σ_r in equations (33) and (38) at $r = a$, thus, from equations (38) and (37):

$$\sigma_r=\sigma_\theta=-\frac{\sigma_0}{\sqrt{3}}\left[2\ln R_0+\frac{2m(R_0-1)}{\rho}+\frac{(1+m)(1-R)}{\rho}\right]-q \quad (39)$$

and

$$\sigma_z=-\frac{\sigma_0}{\sqrt{3}}\left[2\ln R_0+\frac{2m(R_0-1)}{\rho}+\frac{(1+m)(1-R)}{\rho}+\sqrt{3}\right]-q \quad (40)$$

The axial stress in region 2 will be transmitted into region 1 and, unless the length (l) of this region is small, this component of σ_z will be more or less uniform at the punch face, according to St Venant's principle. It may thus be verified that the mean punch pressure is given by

$$\frac{p}{\sigma_0}=\frac{1}{\sqrt{3}}\left[2\ln R_0+\frac{2m(R_0-1)}{\rho}+\frac{1+m}{3\rho}+\sqrt{3}+\frac{2ml}{a}\right]+\frac{q}{\sigma_0} \quad . \quad . \quad . \quad (41)$$

and for the special case of $m = 0$

$$\frac{p}{\sigma_0}=1+\frac{1}{3\rho\sqrt{3}}+\frac{2}{\sqrt{3}}\ln R_0+\frac{q}{\sigma_0} \quad . \quad . \quad (42)$$

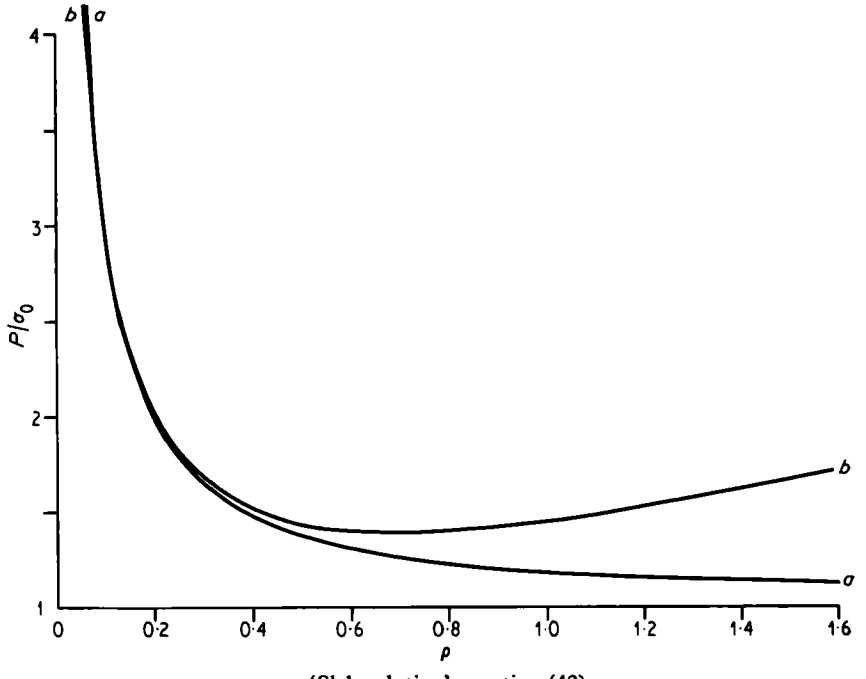

a 'Slab solution' equation (42).
b Optimized upper bound.

Fig. 7. *Comparison of 'slab solution' and optimized upper bound* ($q = 0$)

Equation (42) is similar to equation (22) except that it does not contain the $\rho/\sqrt{3}$ term. This is because the restraining effect of the flange region on axial movement in region 2 has not been accommodated in the simplified equilibrium equations. The punch pressure given by equation (42) is compared with the optimized upper bound in Fig. 7.

If the term in ρ is omitted from equation (42), a lower bound on p is obtained, since without the inclusion of shear on the 1–2 boundary, the Lévy–Mises yield and internal equilibrium equations are satisfied within each of regions 2 and 3 and, because no redundant shearing work occurs in these regions, the deformation is ideal

5 EXPERIMENTAL VERIFICATION OF THE THEORY

Two sub-presses of the type shown in Fig. 8*a* were employed. The illustrated sub-press has a duplex container of 32 mm bore diameter. This is separated from the baseplate by a pair of rectangular bars, a range of which was used to provide different gap heights. The platen is mounted on a piezo-electric load cell of 250 kN capacity, which is used to determine the force transmitted to the platen. With the load cell coupled to a charge amplifier, tests lasting 2–3 min could be performed without measurable zero drift due to charge leakage. The second sub-press (not illustrated) is of essentially similar design except that it has a container of 20 mm bore diameter and a range of interchangeable platens for upsetting flanges part way along the billet. No provision for a load cell is incorporated in this sub-press.

The testing was carried out using a 500 kN Denison hydraulic press, using billets of the following materials: E1c aluminium, in both the annealed and as-received states, copper and an aluminium alloy of unknown composition that was supplied as E1c. This last material proved particularly favourable for etching, to show the flow pattern in deformed specimens. The lubricant used for all the tests was Droyt WS drawing compound.

For the verification of the theory, quasi-static load-punch travel characteristics were obtained by allowing the deforming billet to attain static equilibrium under each of an increasing series of loads before taking readings. This eliminated the effects of strain rate in the materials and also minimized frictional effects. Measurements of the platen force failed to show any difference between that and the punch force during tests on aluminium billets with contact lengths of up to 50 mm in the container bore and punch loads up to 200 kN. The minimum deviation measurable with the load cell connected via a charge amplifier to an oscilloscope would have been 4 kN, which indicates a maximum value for m of 0·05 in equation (24) if 30 MN/m^2 is taken as the initial yield stress of aluminium. As the punch load exceeded 100 kN after very little deformation, it was considered that disregarding frictional effects was justifiable for the purpose of comparing the basic theory with experiment.

Measurement on several products in various stages of deformation showed that the final diameter of the flange could be predicted with less than 3 per cent error from the punch travel values by assuming that the flange profile approximates to the parabolic form shown in Fig. 8*b*. h_0 is taken to be the value expected for an isotropic homogeneous solid, namely $b\sqrt{(1/R_0)}$. It was therefore possible to relate punch pressure directly with R_0 with reasonable accuracy to compare theory and experiment. Comparisons of the experimental results with the optimized upper bound theory are shown in Figs 9–11. σ_{0m} values for the individual tests were derived from true stress–strain curves derived from compression tests on a sample of test material. The value of k in the strain function (equation (30)) was chosen arbitrarily as 0·586, which is such that when $R_0 = 2$, $\phi = 0{\cdot}5$. As is seen from the resulting position of the experimental points relative to the upper bound curves, the experimental points follow the trend of the upper bound quite closely, except at the highest values of ρ. It is also evident that k is (fortuitously, perhaps) very near to the optimum value since the upper bound curves are close to the upward limit of scatter of the experimental points. The lower bound solution (equation (42) without the term in ρ) would in every case underestimate p/σ_0, but this solution is less accurate than the graphs suggest, because use of this solution to calculate

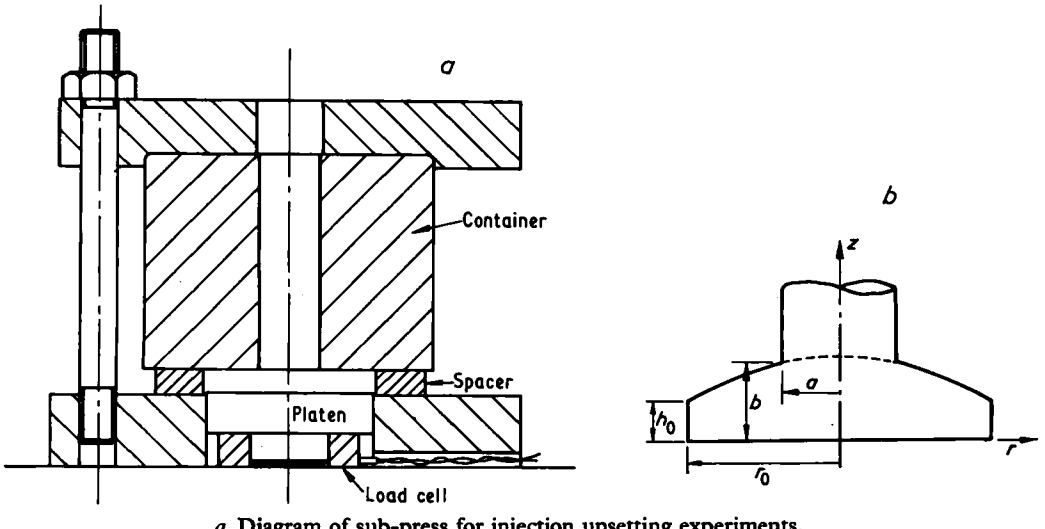

a Diagram of sub-press for injection upsetting experiments.
b Parabolic approximation to flange profile.

Fig. 8

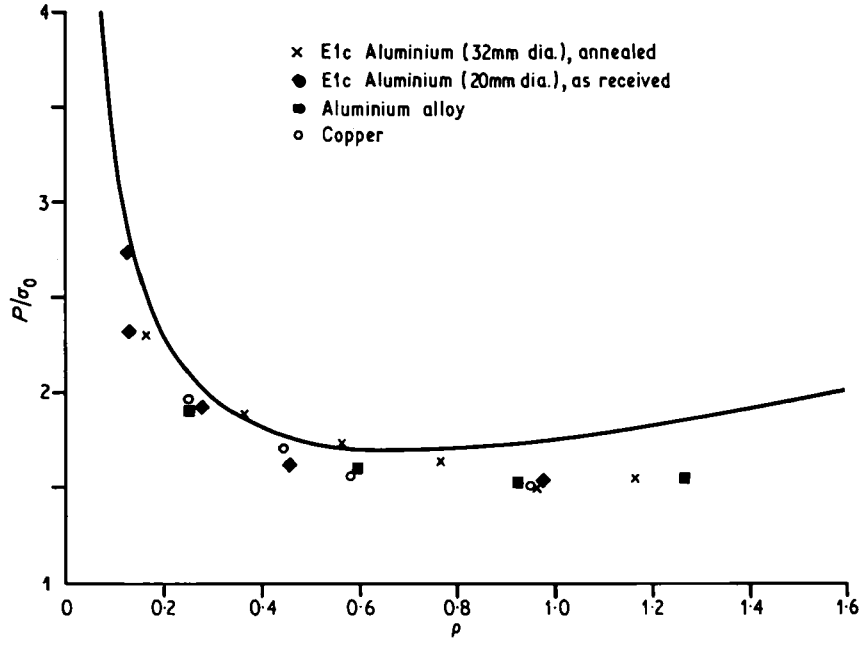

Fig. 9. *Comparison of upper bounds and experimental results for the injection of a flange on the end of a billet* ($R_0 = 1{\cdot}3$)

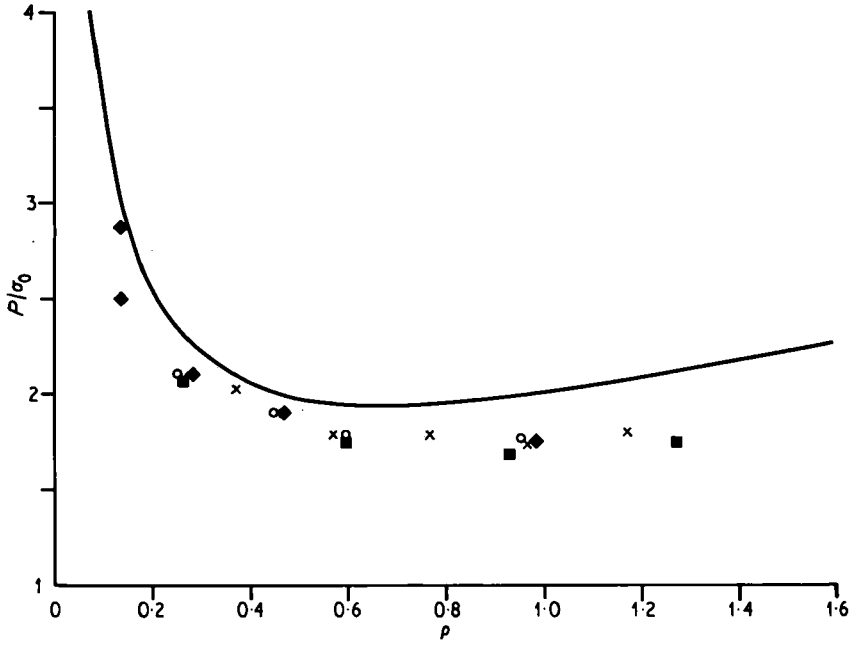

Fig. 10. *Comparison of results for* $R_0 = 1{\cdot}6$

$\bar{\epsilon}_m$ and σ_0 would have the effect of elevating all the experimental points on the graphs.

The same value of k was used to evaluate the theory for injection of flanges part way along the billet (Figs 12 and 13), although the agreement with the upper bound curve is not as good in this case at low values of ρ. This, and the fact that the experimental points do not follow the upward trend of the upper bound curve at large values of ρ suggests that ϕ may be to some extent dependent on ρ. There is, however, an alternative explanation for the behaviour at large values of ρ. The degree of constraint on region 2 is reduced as ρ increases beyond the point at which p/σ_0 is theoretically a minimum. It therefore follows that unless further constraint is applied to region 2 by a bulk of material in region 3 or by an external radial pressure, p/σ_0 cannot increase as ρ increases. This being so, it would be expected that an upward trend of p/σ_0 with ρ might begin to exhibit itself at flange diameters larger than those produced here, provided necking of the flange rim does not occur.

In the upper bound analysis, it was found that the axial extent of the deformation zone (region 2) near the axis is greater than the nominal flange thickness for thin flanges and becomes less than the nominal flange thickness as ρ is increased. This is shown clearly in the etched aluminium alloy specimens of Fig. 14, which also shows that

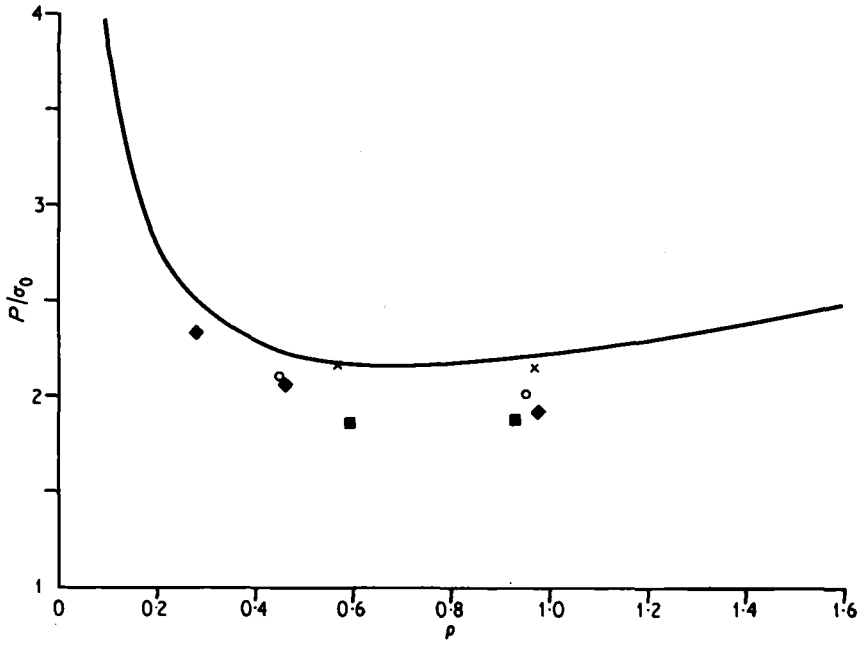

Fig. 11. *Comparison of results for* $R_0 = 1{\cdot}9$

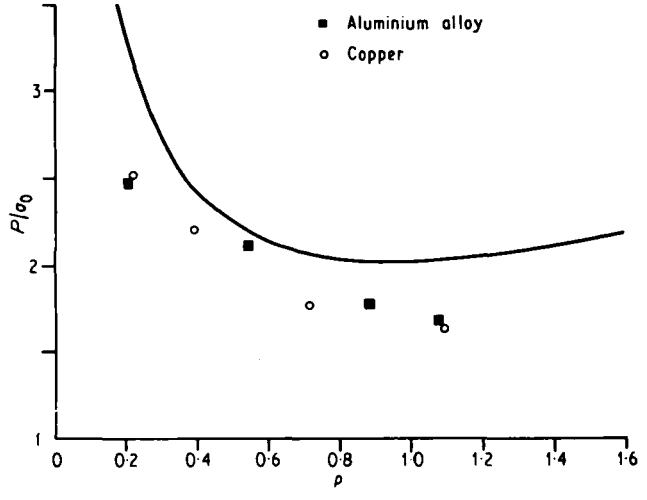

Fig. 12. *Comparison of upper bound and experimental results for the injection of a flange part way along a billet* ($R_0 = 1{\cdot}3$)

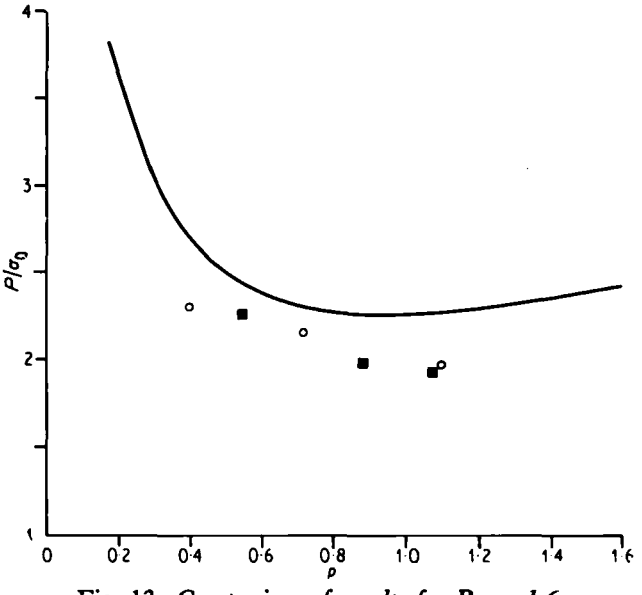

Fig. 13. *Comparison of results for* $R_0 = 1{\cdot}6$

when the lower end of the billet is constrained, the deformation field extends very little into the constrained region and that a surface of heavy shear occurs almost exactly in the plane of the lower flange face in all but one specimen. The elevation of the plane of maximum shear above the flange lower face in the specimen of largest flange thickness reinforces the argument above as to why the observed punch pressures do not follow the upward trend of the upper bound curve for large flange thicknesses. The constraint on the billet is such that an alternative mode of deformation requiring a lower punch pressure is possible and the flow pattern indicates that the billet is tending to deform in region 2 as though ρ were somewhat less than that prescribed by the tool.

6 FORMABILITY OF THE MATERIALS TESTED

In the annealed state, aluminium generally began to show necking at the flange rim when the flange diameter reached twice the billet diameter. If deformation was continued fracture proceeded, from a neck, along a surface inclined at approximately 45° to each principal axis. The as-received aluminium alloy was fairly brittle, but after annealing became similar in formability to the aluminium. Annealed copper was considerably more ductile and could be cold-worked to give flange diameters of three times the billet diameter without necking occurring.

It was generally found that the formability was lower for very thin flanges ($\rho < 0{\cdot}2$) and that it was slightly lower when the flange was formed part way along the billet. It was also found that a small radius (0·1 × billet diameter) at the lower end of the container bore virtually eliminated the scoring of the flange surface which was often prominent in specimens formed with unradiused containers. This radius had the additional effect of reducing by 5–8 per cent the punch pressure required to form a flange of a given diameter. The effect was greatest for the thinnest flanges

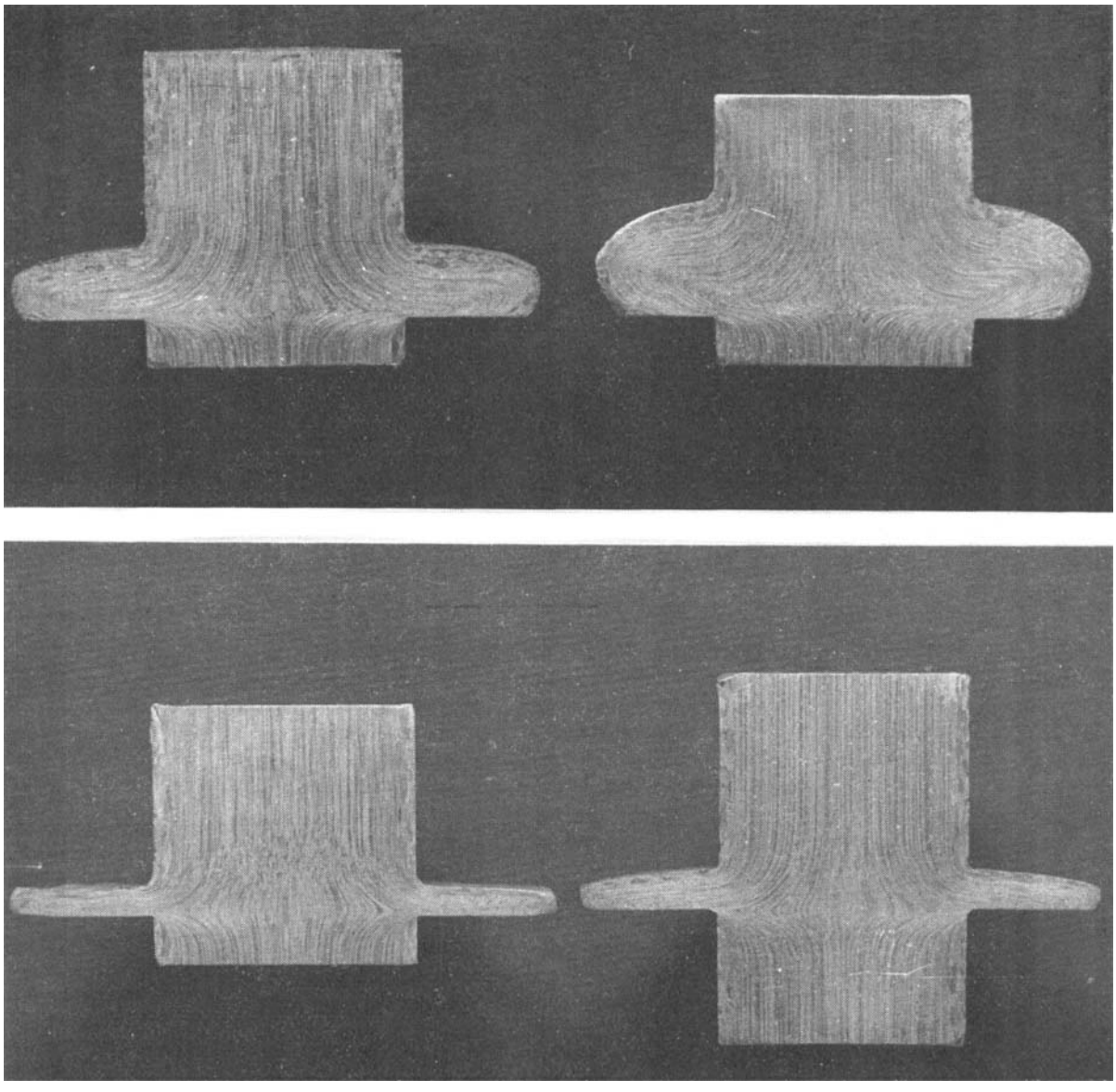

Fig. 14. *Flow patterns in aluminium alloy billets injection upset to give different flange thicknesses*

and is attributable to the modification of the flow field in a region of particularly high redundant strain rate.

7 CONCLUSIONS

While the upper bound solution presented here is an improvement on that of Alexander and Lengyel, its absolute accuracy for an ideal plastic material remains undetermined. It may be noted, however, that replacement of the conical discontinuity surface by a paraboloid produces only marginal reductions in p/σ_0 and these only at the smallest values of ρ. It appears therefore that an appreciable improvement in the theory given here (assuming that it is significantly in error) could be achieved only by making u_r dependent upon z in the deforming region. Experiments using work-hardening materials cannot clarify this matter, firstly because the axial thinning of the flanges will tend to reduce the forming loads (though not greatly) and secondly because of the necessity to introduce the arbitrary work-hardening function ϕ. However, it may be argued that since experiment and theory compare tolerably well and since the upper bound and the work-hardening function are derived from sound principles, the theory should give a reasonable guideline for tool strength requirements for this process. For reasons described above, the stress analysis equation (42) will probably give better estimates of punch pressure requirements for upsetting thick flanges. Since the results for E1c aluminium alloy (as-received) do not differ markedly from the results for annealed materials, it seems that the theory remains applicable when some initial inhomogeneity of yield strength exists within the billet.

APPENDIX 1

DERIVATION OF THE VELOCITY FIELD FOR REGION 2 OF THE DEFORMING BILLET

For continuity of flow from region 1 to a right cylindrical surface of radius r in region 2, it is required that

$$\left.\begin{aligned} U.\pi r^2 &= 2\pi r.u_r\left[\lambda b+\frac{rb}{a}(1-\lambda)\right] \\ \text{i.e.}\qquad u_r &= \frac{Uar}{2b[\lambda a+r(1-\lambda)]} \end{aligned}\right\} . \quad (43)$$

From equation (1):

$$\frac{\partial u_z}{\partial z} = -U\left[\frac{2a^2\lambda + ar(1-\lambda)}{2b[\lambda a + r(1-\lambda)]^2}\right]$$

integrating

$$u_z = -\frac{U_z}{2b}\left[\frac{2a^2\lambda + ar(1-\lambda)}{[\lambda a + r(1-\lambda)]^2}\right] + f(r)$$

where $f(r)$ is a function of r only, which is found from the conditions for continuity of material across the 1–2 boundary. In the notation of Fig. 2*b* this condition is expressed by

$$\left.\begin{aligned} U\cos\phi &= u_z\cos\phi + u_r\sin\phi \\ \text{or} \qquad U + u_z &= u_r\tan\phi \end{aligned}\right\} \quad . \quad (44)$$

Since $\tan\phi = (b/a)(1-\lambda)$, it is found that, from equations (43) and (44), on the 1–2 boundary

$$u_z = -\frac{U}{2}\left[\frac{2\lambda a + ar(1-\lambda)}{\lambda a + r(1-\lambda)}\right]$$

and therefore $f(r)$ must be zero.

Continuity across the 2–3 boundary is automatically satisfied in the above solution and so a kinematically admissible velocity field for the process has been found.

APPENDIX 2

TABLES OF THE FUNCTION $\dot{W}_{12}/(\pi a^2\sigma_0 U)$ FOR VARIATIONS OF ρ AND λ

λ \ ρ	0·06	0·08	0·10	0·14	0·18
0·00	0·578	0·578	0·578	0·578	0·578
0·20	0·682	0·682	0·682	0·682	0·683
0·40	0·773	0·773	0·773	0·774	0·774
0·60	0·855	0·855	0·856	0·856	0·856
0·80	0·931	0·931	0·931	0·931	0·931
1·00	1·000	1·000	1·000	1·000	1·000
1·20	1·065	1·065	1·065	1·065	1·065
1·40	1·125	1·125	1·125	1·125	1·126
1·60	1·181	1·181	1·182	1·182	1·183
1·80	1·235	1·235	1·235	1·236	1·238
2·00	1·285	1·286	1·286	1·288	1·290
2·20	1·333	1·334	—	—	—
2·40	1·379	1·380	—	—	—
2·60	1·423	1·424	—	—	—
2·80	1·465	1·467	—	—	—
3·00	1·506	1·508	—	—	—
3·20	1·545	1·548	—	—	—
3·40	1·582	1·586	—	—	—
3·60	1·619	1·623	—	—	—
3·80	1·654	1·660	—	—	—
4·00	1·689	1·695	—	—	—

λ \ ρ	0·3	0·4	0·6	0·8	1·0	1·2	1·4	1·6
0·00	0·580	0·581	0·586	0·592	0·601	0·610	0·622	0·634
0·10	0·635	0·637	0·643	0·651	0·662	0·675	0·689	0·705
0·20	0·685	0·687	0·694	0·703	0·714	0·727	0·742	0·759
0·30	0·732	0·734	0·740	0·748	0·759	0·772	0·786	0·802
0·40	0·776	0·777	0·783	0·790	0·799	0·810	0·823	0·837
0·50	0·817	0·819	0·823	0·829	0·836	0·845	0·855	0·866
0·60	0·857	0·858	0·861	0·865	0·870	0·877	0·884	0·892
0·70	0·895	0·896	0·897	0·900	0·903	0·907	0·912	0·917
0·80	0·931	0·932	0·932	0·934	0·935	0·937	0·939	0·942
0·90	0·966	0·966	0·967	0·967	0·967	0·968	0·969	0·969
1·00	1·000	1·000	1·000	1·000	1·000	1·000	1·000	1·000

APPENDIX 3

REFERENCES

(1) 'Some aspects of the cold extrusion of steel', N.E.L. Rep. no. 196, 1965.

(2) HENDRY, J. C. 'An investigation of the injection upsetting of six steels', N.E.L. Rep. no. 494, 1971.

(3) COGAN, R. M. 'Hydrodynamic forming', *Machinery* 1964 **105**, 1147–51.

(4) COGAN, R. M. and CAMPBELL, G. L. 'Forging against back pressure', *Am. Machinist* 1963 **107**, 105–7.

(5) COGAN, R. M. and DORMAN, F. S. 'Hydrodynamic compressive forging', General Electric Co. Rep. no. A.S.D. TR 7-890 (III), 1963.

(6) ALEXANDER, J. M. and LENGYEL, B. 'On the cold extrusion of flanges against high hydrostatic pressure', *J. Inst. Metals* 1965 **93**, 137–45.

(7) ALEXANDER, J. M. 'On complete solutions for frictionless extrusion in plane strain', *Quart. appl. Math.* 1961 **19**, 31–7.

(8) BISHOP, J. F. W. 'On the complete solution to problems of deformation of plastic–rigid material', *J. mech. phys. Solids* 1953–54 **2**, 43–53.

(9) HILL, R. 'On the state of stress in a plastic–rigid body at the yield point', *Phil. Mag.* 1951 **42**, 868–75.

(10) JOHNSON, W. 'Estimation of upper bound loads for extrusion and coining operations', *Proc. Instn mech. Engrs* 1959, **173**, 61–72.

(11) KUDO, H. 'An upper bound approach to plane strain forging and extrusion' (in 3 parts), *Int. J. mech. Sci.* 1960 **1**, 57–83, 229–52 and 366–8.

(12) KUDO, H. 'Some analytical and experimental studies of axisymmetric cold forging and extrusion' (in 2 parts), *Int. J. mech. Sci.* 1960 **2**, 102–27 and 1961 **3**, 91–117.

(13) AVITZUR, B. *Metal forming: processes and analysis* 1968 (McGraw-Hill, New York).

(14) THOMSON, E. G., YANG, C. T. and KOBAYASHI, S. *Mechanics of plastic deformation in metal processing* 1965 (Macmillan, New York).

(15) AVITZUR, B. 'Limit analysis of disc and strip forging', *Machine Tool Des. Res.* 1969 **91**, 165–95.

(16) MILNER, P. R. 'The injection upsetting process', Ph.D. Thesis, The University of Leeds, 1971.